Parametric assessment of a portable hydrokinetic turbine through numerical simulations and experimental set-up

Avaliação paramétrica de uma turbina hidrocinética portátil através de simulações numéricas e montagem experimental

A. M. A. Pinto[1,3] | R. M. A. Pedroso[3] | S. I. S. Pinto[1,2,(*)]

[1] Engineering Faculty, University of Porto, Porto, Portugal
[2] Institute of Science and Innovation in Mechanical and Industrial Engineering (LAETA-INEGI), Porto, Portugal
[3] Centre of Nanotechnology and Smart Materials (CeNTI), Vila Nova de Famalicão, Portugal
[(*)] *Email:* spinto@fe.up.pt

abstract

The present study aims to explore, develop, and optimize a portable hydro turbine capable of harnessing energy from rivers and canals. To maximize energy extraction and achieve high power coefficients, horizontal axis hydrokinetic turbines were selected. Within this study, diverse turbine models were created using the *QBlade* software, based on *Blade Element Momentum* (BEM) theory. Furthermore, the feasibility of implementing a diffuser around the turbine was investigated. The performance evaluation of the hydrokinetic turbine was conducted using a numerical CFD model. With the final diffuser, the turbine exhibited a maximum power coefficient of 66.5%, further validated through experimental testing.

Keywords: turbine, diffuser, torque, energy efficiency, CFD, experimental set-up

resumo

Este estudo tem como objetivo explorar, desenvolver e otimizar uma turbina hídrica portátil capaz de aproveitar a energia de rios e canais. Para maximizar a extração de energia e alcançar altos coeficientes de potência, foram selecionadas turbinas hidrocinéticas de eixo horizontal. Dentro deste estudo, diversos modelos de turbinas foram criados usando o *software QBlade*, baseado na teoria BEM (*Blade Element Momentum*). Além disso, foi investigada a viabilidade de implementação de um difusor em torno da turbina. A avaliação do desempenho da turbina hidrocinética foi realizada utilizando um modelo numérico de CFD. Com o difusor final, a turbina apresentou um coeficiente de potência máxima de 66,5%, mais tarde validado por meio de testes experimentais.

Palavras-chave: turbina, difusor, torque, eficiência energética, CFD, montagem experimental

1- INTRODUCTION

The issue of global warming has gained widespread attention in recent decades, as the devastating impacts of climate change become increasingly evident, creating a pressing need to switch to renewable energy sources that are sustainable, reliable, and have a low environmental impact [1]. Amidst a range of renewable energy sources available, hydro, solar, and wind power have emerged as promising alternatives to fossil fuels. Hydropower has gained significant attention due to its potential as a reliable and sustainable energy source. The use of this renewable source to produce electricity is an established activity with well-developed technologies [2]. Hydropower constitutes approximately 20% of the global annual electricity generation and in many countries, it is the only domestic source of electricity generation [1]. In Portugal, the increased use of endogenous and renewable resources for electricity production has transformed the production mix and played a critical role in meeting energy consumption.

Like most renewable sources, hydropower is an indirect form of solar energy. Part of the incident solar radiation is consumed by the evaporation process, therefore, the water vapor in the atmosphere represents an accumulation of huge amounts of energy that can be harnessed later as a result of the precipitation that happens in the highlands [2]. To capture this energy, there are five main types of hydropower systems according to the technology used: Conventional hydropower plant - Large dams across rivers that produce electricity by converting the potential energy of a watercourse; Run-of-river - Weir structures that divert a fraction of a river's water flow towards a turbine, to generate electricity; Pumped-storage - Water is pumped from a lower reservoir to a higher reservoir during periods of low electrical demand, boosting the potential energy; In-stream - Installing hydrokinetic turbines in the stream of rivers to generate energy; Gravitational Vortex Plant - Use the vortex's energy to produce electricity [3].

In order to extract the energy inherent in water, either in the form of potential or kinetic energy, it is necessary to convert it into mechanical energy, and subsequently, into electricity. To do this, the use of a turbine and a generator is needed, respectively. The water flow spins the turbine that is coupled to a mechanical shaft, which in turn is linked to the generator shaft. Therefore, the selection of any type of hydro turbine and respective generator is crucial for a project.

Depending on how they use the energy contained in the flow, turbines can be classified into three main types: Impulse - The water is directed onto a set of blades using injectors, that convert the pressure into kinetic energy through area variation; Reaction - Combined action of pressure difference and kinetic energy when fully submerged and enclosed in a spiral case; Kinetic/Free-flow - Harness the kinetic energy from the flowing water without the need for a head difference, in contrast to previous ones [1]. As this project aims to design and optimize a portable hydroelectric turbine, that is able to fit into a hiking backpack and produce electricity directly from a watercourse, the hydrokinetic turbine turned out to be the best suitable for the application due to its simplicity and versatility. Hydrokinetic energy is one of the renewable energies that has garnered substantial global attention on a worldwide

scale, primarily attributable to its reliability, uninterrupted availability, sustainability, and elevated energy density. The accessibility of long rivers with reliable and high flow rates in many countries, substantially increases the viability of this technology, showing enormous potential for its implementation [4]. Its ineffective conversion efficiency is the main issue in this area. Enhancing the performance of hydrokinetic turbines is still a challenge for engineers [5]. The hydrokinetic turbine, also called a free-flow turbine, is a device that uses the stream flow of water to turn the turbine blades, in order to capture the kinetic energy of the fluid. Pressure differences created between the upstream and downstream portions of the blades provide the rotational motion, instigating the transformation of kinetic energy inherent in water flow into mechanical work.

In hydrokinetic turbine design, two main categorizations emerge: the horizontal axis (HAHT) and vertical axis (VAHT) hydrokinetic turbine. The former configuration entails an orientation where its rotational axis is parallelly aligned with the vector of incoming velocity, operating under theoretical conditions. In contrast, the latter has its axis oriented perpendicular to the incoming velocity. The low starting torque and inherent self-starting capabilities of axial-flow/horizontal turbines are just two of their many noteworthy benefits in comparison to VAHTs. Worth mentioning that HAHTs are lift-based which would translate into a smaller anchoring force in axial turbines, leading to a diminished total mass [6]. Therefore, it was found that the horizontal axis turbine design was the ideal orientation for this project due to its more straightforward construction and functional attributes that complemented design objectives. Conversely, these turbines present more complicated design issues since maximizing efficiency necessitates a correct distribution of twisting angle and chord dimension along the blade span [6]. Focusing on the horizontal axis hydrokinetic turbine, some developments have been made by engineers, however, remain one of the primary untapped resources. *Marina et al.* [7] optimized a rotor blade design, aiming to get as close as possible to the efficiency limit known as the *Betz Limit*. The optimization process was based on classical *Blade Element Theory*, for the design blades of the hydrokinetic turbine [7]. *Ion et al.* [8], [9], [10], [11], [12] produced power and torque curves for a conventional kinetic turbine configuration in order to evaluate its performance. Significant enhancement in the power output of horizontal-axis hydrokinetic turbines was achieved through the utilization of various shroud/diffuser geometries, as reported in [7], [13]. This improvement in power extraction from the flow consequently increased the power coefficient value, most of the time even exceeding the *Betz Limit*. Regarding computational fluid dynamics simulation, *Marina et al.* [7] use the software package *FLUENT* from *ANSYS* to perform the analysis and obtain the required turbine parameters. The findings of *Marina et al.* [7] further affirm that, regardless of the particular turbine set-up, the application of elongated diffusers and elevated expansion angles leads to an increase in water velocity at the rotor plane. *W. Schleicher et al.* [14] provides insight into the computational models that were utilized to assess the design. An investigation was made particularly in the domain specification and in the generating mesh for CFD analysis [14]. The validation undertaken by *Gish et al.* [13] involved an experimental arrangement incorporating components such as a tachometer, a torque meter, and a voltage brake utilized for generating a variable resistance load, creating a performance curve based on the power output from the prototype unit. Blue

Freedom [15] and Seaformatics [16] offer two primary models of low-power portable turbines for commercialization. Both are intended to be tethered with a cable immersed in a flowing water source, aiming to harness kinetic energy for charging batteries or small portable electronic devices.

Once the main limitation is the turbine size, the goal of the present study is to maximize the power generated while keeping the scale of the system relatively small with minimal weight. Through this process, it is expected to: Conduct an intensive overview of the current state of hydro turbine technology to best choose the type for the portable turbine; Analyze types of equipment that can be useful to implement in the design prototype; Optimize the turbine rotor based on the *BEM Theory*; Develop a numerical model of the hydrokinetic turbine, and test it for a steady state regime, under project conditions; Use advanced computational tools, such as CFD (Computational Fluid Dynamics) software, to simulate and improve the hydro turbine design in order to increase its output power and efficiency; Fabricate and assemble the optimized turbine to verify its performance and validate the numerical model.

2- MATERIALS AND METHODS

2.1. Numerical methodology

2.1.1. Turbine

Design procedure

The turbine's design was modeled within the *QBlade* software, a strategic choice made to expedite computational processes. By incorporating the *Blade Element Momentum* (BEM) theory, which is integrated into *QBlade* package, a more time-efficient approach was adopted. This software package is interfaced with the *XFOIL* computational tool, facilitating the expeditious generation of hydrofoil geometries and computing their lift-drag polar extrapolated across a full 360-degree angle of attack range. For the design of the rotors, in order to acquire the one with the best performance, beyond optimization through BEM theory for each blade design, the hydrofoil and hub designs were varied in order to obtain the final prototype of the bare turbine. Eppler 817 (E817) and Selig / Giguere SG6043 were the hydrofoils analyzed in this study.

Subsequently, by specifying the Reynolds number to simulate the flow around the hydrofoil, the lift-drag polar was established, thus capturing its aerodynamic performance across a range of angles of attack. The lift coefficient curve and the drag coefficient curve are typically included in the polar. The Viterna-Corrigan post-stall model, favored in industrial environments, was chosen for this procedure. After this stage, within the design module, the optimized rotors were created. While devising these designs, specific parameters, as outlined in Table 1 were maintained as constants.

Table 1 | Predefined parameters for turbine design.

Parameters	Constant values
Free-stream water velocity (V_∞)	1.0 m/s
Number of blades (B)	3
Water density (r)	998.2 kg/m^3
Turbine radius (R)	0.1 m
Hub radius (r_0)	0.015 m
Reynolds number (Re)	160000
N_{crit}	4

The free-stream water velocity adopted was chosen considering the rivers' typical water flow. A conservative estimate of 1 m/s shall be used out of caution and to prevent overestimating flow energy. For each rotor, the number of blades, B, was set to three. Typically, turbine systems employ three blades to maintain dynamic balance and minimize the fatigue effect. Also, the turbine rotor and hub diameter must be specified. The former was fixed to 20 cm by design constraints, and the latter will equal 15% of the turbine diameter, in accordance with the recommendations outlined in [4]. The water properties used to calculate the Reynolds number were taken from the *ANSYS* database. Last but not least, the user-defined parameter N_{crit}, implemented in *XFOIL*, represents the logarithm of the amplification factor connected to the most amplified frequency that triggers transition. The specific value of N_{crit} depends on the level of ambient disturbance and it simulates how these disturbances affect the transition process [17]. A N_{crit} of 4 was considered a suitable value for replicating the operational conditions and was used from this point forward [17].

The blade profile was divided into 33 positions along the blade length characterized by its position (distance from the turbine center), chord length, twist angle, hydrofoil type, and its corresponding 360º polar plot [18]. Firstly, the tip speed ratio (TSR), given by Equation (1), for which the turbine is optimized has to be defined.

$$TSR = \frac{\omega R}{V_\infty} \tag{1}$$

where ω is the angular velocity, R is the turbine radius and V_∞ is the free-stream velocity. Hydrokinetic turbines are carefully designed with an optimal tip speed ratio to maximize power extraction. If the purpose of the technology is to extract energy from the moving water, like hydrokinetic turbines, the theoretical power available, P_{Theo}, can be expressed as Equation (2).

$$P_{Theo} = \frac{1}{2}\rho A_{turb} V_\infty^3 \tag{2}$$

where A_{turb} is the turbine's area facing the flow. However, this scenario is not physically feasible and only a fraction of the kinetic energy present in the water passing through the turbine cross-section can be harnessed. The kinetic energy fraction that the turbine captures can be expressed using the power coefficient, C_P. Equation (3) gives the actual power that the turbine can extract from the watercourse [5], after accounting for losses and inefficiencies P_{Real}.

$$P_{Real} = \frac{1}{2} C_P \, \rho A_{turb} V_\infty^3 \, \eta_r \tag{3}$$

where η_r is the product of the efficiencies of the generator, transformer, and other electrical components. On the contrary, the *Blade Element Momentum* (BEM) theory evaluates the contribution to the total power *dP*, considering the flow through an annular cross-section of radius *r* with area 2*prdr*, as the infinitesimal torque (*dM*) times the rotor angular velocity, as shown in Equation (4).

$$dP = \omega dM \tag{4}$$

Thus, the total power generated from the rotor can be obtained from Equation (5).

$$\mathrm{P} = \int_{r_0}^{R} dP \; dr = \int_{r_0}^{R} \omega dM \; dr \tag{5}$$

being r_o the hub radius. For low *TSR* values, the turbine will tend to slow or stall, while for high *TSR* values, the turbine will rotate too quickly to extract power and will be stressed and may structurally fail. Consequently, selecting the right *TSR* ensures that the turbine operates optimally.

Given the considerations, a *TSR* value of 1 was fixed for all the designs, which led to an optimal rotational speed of 10 rad/s. Subsequently, the glide ratio was used for optimizing the twist angle. This ratio is the quotient between the lift and drag coefficients. Optimize for lift-drag ratio sets the twist angle to an incidence angle that yields the highest glide ratio. Finally, the chord distribution was optimized according to *SCHMITZ* whose equation can be found in [18].

The *AoA* that corresponds to the maximum value of the glid ratio was the angle introduced in *QBlade* to optimize the twist angle. The Eppler 817 was the first hydrofoil tested and incorporated in a blade cross-section design. For this, the design *AoA* was 4º and the SG-6043 hydrofoil was tested for a design *AoA* of 4.25º.

The glide ratio of the hydrofoil is only one of several variables that might affect the operation of the turbine. It is crucial to acknowledge that the turbine performance depends on various other parameters. Consequently, the design *AoA* considered previously may not necessarily yield optimal turbine performance under the designated conditions. An *AoA* of 0º was considered, as this aids in preserving laminar flow along the blade surface which can reduce drag and improve overall efficiency. Experimental testing and computational fluid dynamics (CFD) simulations can be useful techniques for maximizing turbine performance and choosing the best design parameters for a particular application.

Geometric models

This section presents the models for the turbine geometries analyzed. After finishing the design process, the blade geometry obtained can be exported in STL file format from *QBlade* software. However, this turned out to be a challenge as the exported file consistently damaged the blade geometry. To solve the problem, all rotor designs were performed using the results of chord length and twist angle. Figure 1 shows the geometries performed with the CAD tool investigated in this study.

The designs created with the Eppler 817 hydrofoil, APFEUP1 and APFEUP2 models, were designed for an *AoA* of 0º and 4º angle of attack, respectively. The APFEUP3 and APFEUP4 models were designed with SG-6043 hydrofoil with an *AoA* of 0º and 4.25º, respectively. Alternative

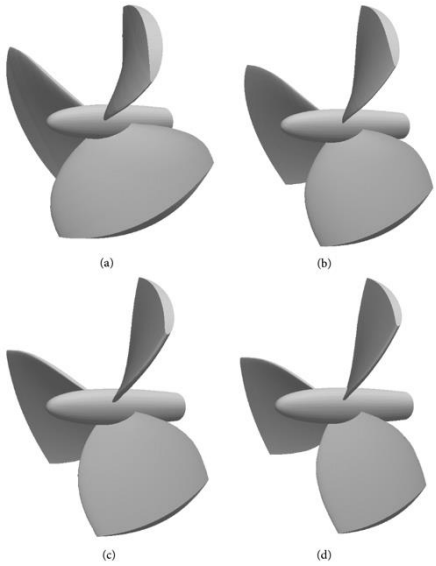

Fig. 1 | Turbine models. (a) APFEUP1. (b) APFEUP2. (c) APFEUP3. (d) APFEUP4.

angles of attack (*AoA*) were examined within the *QBlade* software to refine the blade design. However, the differences do not justify CFD simulations, based on the BEM Module analysis. It is worth noting that a consistent hub design was applied to all previous geometries, ensuring that the turbine's efficiency is unaffected and solely reliant on the blade design.

Numerical procedure

Once obtained the turbine's design, the numerical simulations pertinent to this study were executed using the *FLUENT* software package, a component of *ANSYS* R1 2023, which employs the Finite Volume Method (FVM) for the resolution of numerical equations. Saving the turbine's 3D CAD model as a STEP file, the subsequent step involved importing the geometry into *SpaceClaim*, a design software available from *ANSYS Workbench*. With this tool, a computational set-up was performed. Within the computational domain, two distinct cylindrical domains were defined: the first corresponding to the rotating region and the second representing the stationary zone. Figure 2 shows the computational set-up created for the CFD simulations.

The computational mesh was generated using Meshing Ansys®. Two parameters must be evaluated to attain a mesh with good quality elements and the most suitable to achieve accurate results. Tetrahedral elements were chosen to apply a method to uniform the elements and avoid agglomeration of elements, and consequent increase of elements number, in unnecessary regions.

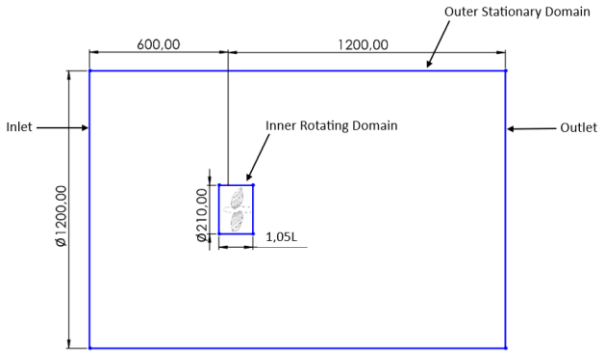

Fig. 2 | Computational set-up (dimensions in millimeters).

The diameter and length of the inner rotating zone were both increased by 5% relative to the rotor diameter (D) and the hub extent, respectively. Subsequently, the turbine body was extracted from the inner cylinder obtaining only the domain around the CAD geometry. This configuration enabled the simulation of the rotating fluid. In the outer part, a $6D$ diameter was set. For the downstream length, the same length was considered ($6D$), from the turbine origin, to consider the wake effect. Finally, a $3D$ upstream distance was used [19].

The subsequent procedural phase involves mesh generation, which is executed through the utilization of *ANSYS Fluent Meshing*. It is necessary to discretize the governing equations that describe fluid motion in the computational domain. Given the intricate nature of these equations, it is unfeasible to solve them analytically for complex flows. To ensure a faithful depiction of the underlying physical phenomena in fluid dynamics simulations, it is imperative to employ a suitable mesh since it affects how accurate the results are. Thus, in areas where larger velocity gradients are expected (near the walls and interface zones), the mesh should be refined. Subsequent to the completion of mesh generation, the numerical analysis can be carried out using the *ANSYS FLUENT* module. Accordingly, the boundary conditions of the computational domain were specified to mimic the real conditions. Finally, to calculate and obtain the flow properties, the flow governing equations must be solved. Furthermore, given the inherently turbulent nature of the flow around the turbine, the incorporation of a turbulence model becomes imperative, introducing supplementary equations. For this project, the *SST* k-ω turbulence model was used as in [7]. Thus, two new equations are inserted, one for turbulent kinetic energy k and another for turbulent dissipation rate ω, which govern the energy associated with turbulence and regulate the turbulence scale, respectively [7]. To account for the effect of the turbine rotation, the rotating reference frame was incorporated in the inner domain. Adopting this process, it is possible to define the angular velocity for the rotating domain.

The turbine's torque can be calculated by integrating the pressure and viscous forces acting on the turbine blades. With *FLUENT*, a report was generated to obtain the turbine's torque. It is important to highlight that all simulations conducted within this project will be in a steady-state regime, as the goal is to acquire data for the turbine operating at a constant angular velocity.

Mesh convergence study and mesh quality

In the ideal mesh, precision and computation time should be balanced. To accomplish this, one of the simulated geometries was chosen, and the element sizes were systematically altered. The model APFEUP1 was used to conduct the grid dependency test. This mesh study was done for an angular velocity of 100 rpm to obtain the resultant extracted power. Figure 3 demonstrates the influence of the number of elements in the mesh.

Thus, conducting an analysis and performing a comparison of the power output results enables the identification of a threshold point beyond which minimal variation occurs, as the mesh is refined. A difference of 0.5% and 0.2% was noted between the mesh with 5.2 million elements and the meshes with 7.2 and 12.6 million elements, respectively. The observed disparity is deemed tolerable given the association between the number of elements and the corresponding increase in computational time, leading to the choice of the mesh with 5.2 million elements as the most practical option.

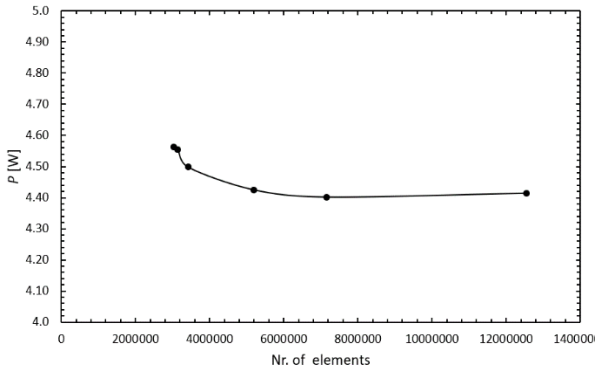

Fig. 3 | Model APFEUP1 grid dependency test evaluating the power output to an angular velocity of 100 rpm varying the number of elements. Window visualization for power output between 4 W and 5 W.

Power vs. angular velocity curve

Something that will not be analyzed exhaustively in the present work will be the choice of the generator since the main objective is the turbine design. However, the selection of the generator dictates the eventual power output that will be used. In a steady-state regime, the resistive torque imposed on the turbine shaft by the generator's magnetic field will equal the induced torque in the turbine, ensuring a constant rotational speed. As a result, the turbine will rotate at the angular velocity dictated by the resistive torque. This curve, which will be generated for all the examined designs, exhibits two points of zero power and a peak power that represents the optimal operating point for which the turbine generates the maximum power output.

2.1.2. Diffuser geometry

In this work, an investigation was conducted to explore the feasibility of overcoming the theoretical efficiency limit, the *Betz Limit*, with the implementation of a diffuser.

Geometric models

This section provides a comprehensive exposition of all the evaluated diffuser designs, presented in Figure 4. The first configuration studied was adapted from [7], the DFB-3 design. Taking this into account, the DFBRIM-FEUP diffuser, shown in Figure 4a, was created. A divergent profile is normally used for the diffuser's shape as it normally increases the water velocity. The DFBRIM-FEUP diffuser contains a brim/flange at the divergent exit with the intention of increasing its efficiency. The following three diffusers tested were adapted from [20] creating the models shown in Figures 4b to 4c. The procedure followed to design the DFNACA diffusers presented in this project, which was based on the approach presented by [20], consists on, design the NACA 0015 hydrofoil and rotating counter-clockwise each point, through a linearly varying angle, around the leading edge. This means a rotation of 0º at the leading edge and 8.08º at the trailing edge. Between these extreme points, the rotation varies linearly with the position. Finally, a full-body clockwise rotation was imposed on the obtained cross-section [20]. This final step was the only difference between the two DFNACA diffuser types. Figure 4b shows the DFNACA10 diffuser. As the name suggests, a 10º rotation was performed in the last step of the procedure. Figure 4c displays the DFNACA20 diffuser. Evidently, this design was built with a 20º rotation. Figure 4d shows the first of two models that were created to outperform the previous designs. The DFAP1-FEUP model was designed based on a combination of a converging inlet, a diverging outlet, and

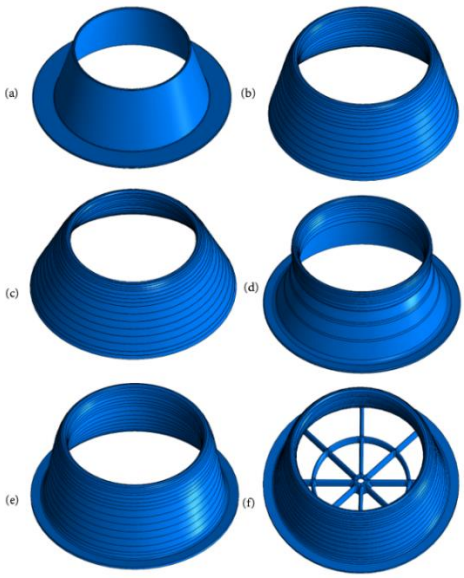

Fig. 4 | Diffuser models. (a) DFBRIM-FEUP. (b) DFNACA10. (c) DFNACA20. (d) DFAP1-FEUP. (e) DFAP2-FEUP. (f) Support structure.

DFNACA10-FEUP diffuser. Building upon the convergent-divergent design, the convergent portion was modified by incorporating the initial half of the cross-sectional profile employed in model DFNACA10-FEUP. The second innovative diffuser is illustrated in Figure 4e. Is notorious the similarity between this and the DFNACA10-FEUP model. The distinguishing feature of the DFAP2-FEUP design is the incorporation of a brim at the divergent exit. Across all the designs, the inlet diameter remained consistent at a value corresponding to 1.2 *D*. The diffuser width and outlet diameter used in almost all models were respectively 0.75 *D* and 1.75 *D*, defined due to portability constraints. To accommodate and fix the turbine at the center of the diffuser, a support structure was designed with an aerodynamic cross-sectional profile, aiming to minimize its interference with the flow while maintaining the structural integrity of the support itself. Thus, the diffuser exhibiting the best performance characteristics was customized to fit this support structure and subsequently subjected to further Computational Fluid Dynamics simulations. Figure 4f exhibits the support configuration employed within the diffuser. It is pertinent to highlight that, in the case of the turbine exhibiting the best results, the position and length of the hub within the diffuser were systematically adjusted with the objective of enhancing the overall performance of the turbine-diffuser assembly. However, no significant improvement was achieved, compared to the initial assumption of vertically aligning the "nose" of the turbine with the diffuser inlet. As a result, the corresponding results will not be included in this paper, as per the author's discretion.

Numerical procedure

Assembling the diffuser with the bare turbine (turbine "nose" aligned with the diffuser inlet), and saving it as a STEP file, allowed to import the geometry into *SpaceClaim* and create a similar computational set-up as mentioned in section 2.1.1. In this scenario, the diffuser will be encompassed within the outer domain, or, for better understanding, the total volume of the diffuser geometry will be removed from the liquid volume attributed to the outer domain, employing an identical methodology applied previously to the bare turbine. Regarding the meshing aspect, an analogous process to the one described in section 2.1.1 was employed, including appropriate sizing criteria for the diffuser walls.

A mesh convergence analysis was performed to validate the mesh parameters and will be carried out immediately. The subsequent steps will be excluded based on their resemblance to the numerical methodology executed for the bare turbine. A numerical analysis was also executed on the diffuser itself in order to enable the visualization of the velocity profile internally. Obviously, in this case, only the outer domain was generated, and again, a similar process to section 2.1.1 was implemented.

Mesh convergence study and mesh quality

A mesh dependency test was conducted for the APFEUP1 + DFBRIM-FEUP model to ensure an adequate mesh to run the simulations. Similar to the previous mesh analysis, this study was conducted at an angular velocity of 100 rpm. Figure 5 elucidates the influence of modifying the number of elements on the obtained results.

In contrast to the turbine study, there is no remarkable variation in the power results as the number of elements increases. As shown in Figure 5, all the points converge around a mechanical power output of 8.25 W with a difference of 1.7% between the mesh with 6.2 million elements and the finest mesh arrangement (24.4 million elements). For the same reasons as the turbine's case, the mesh chosen was the one with 6.2 million elements.

2.2. Experimental methodology

2.2.1. Experimental set-up

A laboratory configuration was constructed to evaluate the accuracy of the CFD numerical model and verify its predictions. In order to validate the CFD model, the power vs. angular velocity curve will be replicated using the Turbine + Diffuser most efficient combination, according to the simulations. Testing was conducted in a 40 m water channel at FEUP, in the Department of Civil Engineering. The discharge of water from the water channel is propelled by three powerful pumps, which transfer it to an upper reservoir where gravitational forces redirect it back into the channel. Therefore, the flow rate in the channel is contingent upon the pumps' capacity to maintain a sufficient water level in the reservoir. The maximum possible flow rate within the channel was regulated by two electromagnetic flowmeters, to be 70 m^3/s. The maximum water velocity in the channel can be obtained by dividing the maximum flow rate by the immersed cross-sectional area. In this case, the water velocity at which it will be possible to test the prototype is approximately 0.12

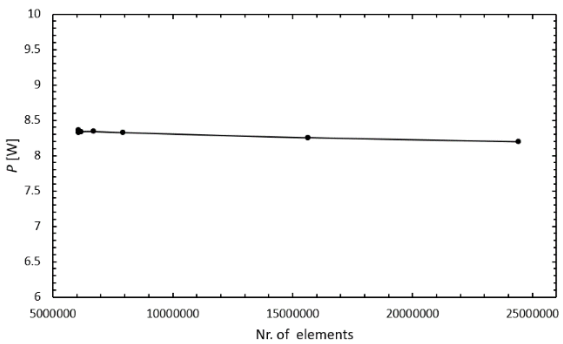

Fig. 5 | Diffuser models. (a) DFBRIM-FEUP. (b) DFNACA10. (c) DFNACA20. (d) DFAP1-FEUP. (e) DFAP2-FEUP. (f) Support structure.

m/s. However, due to the non-ideal nature of the channel, a measurement of water velocity at the turbine inlet will be conducted using a Nortek Vectrino. The acquired water velocity registered a magnitude of 0.11931 m/s. Since the turbine has been optimized to extract energy in flows with water velocities of 1 m/s, replicating the precise design conditions studied is not feasible. However, despite this limitation, a power vs. angular velocity curve will be acquired either experimentally in the available channel and, by employing the same CFD model, adjusted to match the channel water velocity. These results will be subsequently compared.

The turbine and diffuser assembly will be placed inside the channel, supported by a metallic framework that houses a set of bearings and two polymeric bevel gears. These components will enable the conversion of horizontal axis rotational motion into vertical axis motion. Furthermore, a wire will be attached to the vertical rotation axis at one end and connected to a mass M at the other end. The schematic representation of the complete assembly to be constructed is illustrated in Figure 6.

This approach was employed to emulate the action of the generator on the turbine shaft, aiming to minimize the expenses associated with measuring the requisite parameters for obtaining the power vs. angular velocity curve. By varying the mass, the torque can be adjusted, with its magnitude determined by the product of the gravitational force exerted by the mass M and the radius of the shaft. The angular velocity values were measured through an optical tachometer. Consequently, all the requisite parameters will be available to obtain the power vs. angular velocity curve. Regarding the experimental methodology, the resistive torque was initially set at a low value, achieved by using a low/null mass (resulting in a high angular velocity). The resistive torque was then gradually increased until the turbine experienced a stall condition.

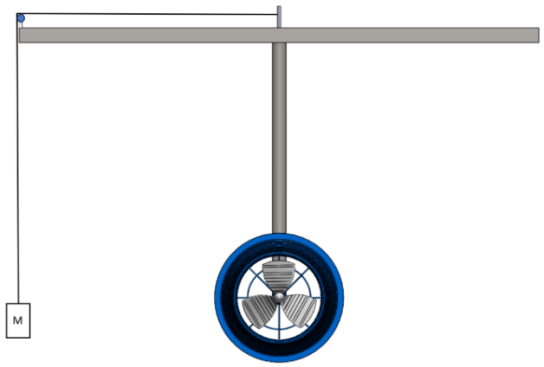

Fig. 6 | Model of the final experimental set-up.

2.2.2. Model construction

The subsequent phase entailed the fabrication of the final model, wherein 3D Fused Deposition Modeling (FDM) on CeNTI's XPIM POM machine was selected for the turbine and diffuser manufacture. PLA polymer was chosen as the material due to its favorable printing characteristics and its greater accessibility in comparison to other materials. The support structure for both the diffuser and turbine was constructed using steel. The two tubes accommodating the rotation shafts possessed an outer diameter of 38 mm and the horizontal bar had a 40 mm edge. The rotation shafts, with a diameter of 10 mm, were supported by four 6300-2RS bearings, with two bearings assigned to each shaft. The two bevel gears inside the

steel elbow were 3D printed using PLA material. Subsequent to the complete assembly of the various components, the set-up was fixed in the water channel to carry out the necessary experimental tests. Figure 7 shows the installation of the structure on the water channel.

As the turbine rotates, the wire progressively wraps around the shaft, inducing the elevation of the mass. The gravitational force acting on this mass contributes to the emergence of the resistive torque.

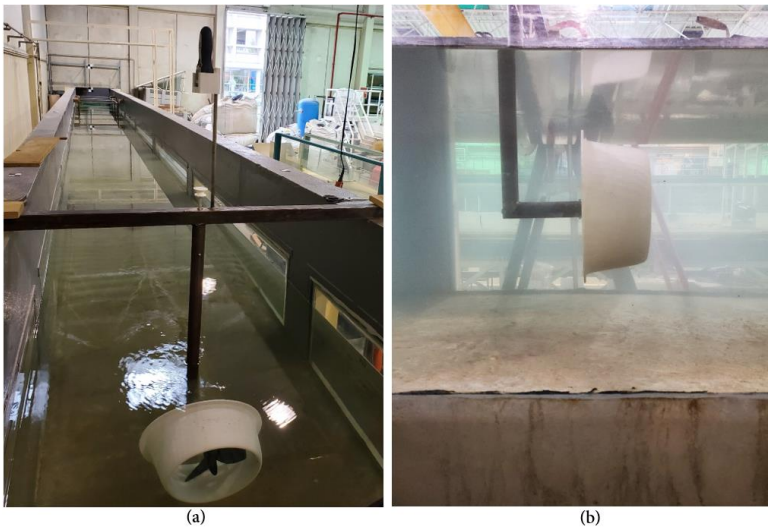

Fig. 7 | Experimental set-up. (a) Front view. (b) Side view.

3- RESULTS AND DISCUSSION

3.1. Numerical simulations

3.1.1. Turbine

Firstly, the performance of the designed turbines was conducted employing the computational fluid dynamics (CFD) model. Figure 8 illustrates the pressure distribution around the bare turbine (model APFEUP3), for an angular velocity of 100 rpm. The selection of this model was made based on the author's judgment, considering that incorporating all models could potentially overwhelm the reader's analysis. From the frontal view in Figure 8a, it is evident the formation of regions characterized by low and high pressure on opposite sides of the turbine blade, that will induce rotational motion to the turbine. This observation aligns with the anticipated outcome, as the turbines were designed to operate based on lift forces. On the other hand, observing the side view in 8b, an increase in pressure can be observed upstream of the turbine, followed by a sudden decrease in this pressure downstream of the rotor. Subsequently, the pressure is then recovered to the free flow pressure. Figure 9 shows the velocity distribution around the rotor, for an angular velocity of 100 rpm.

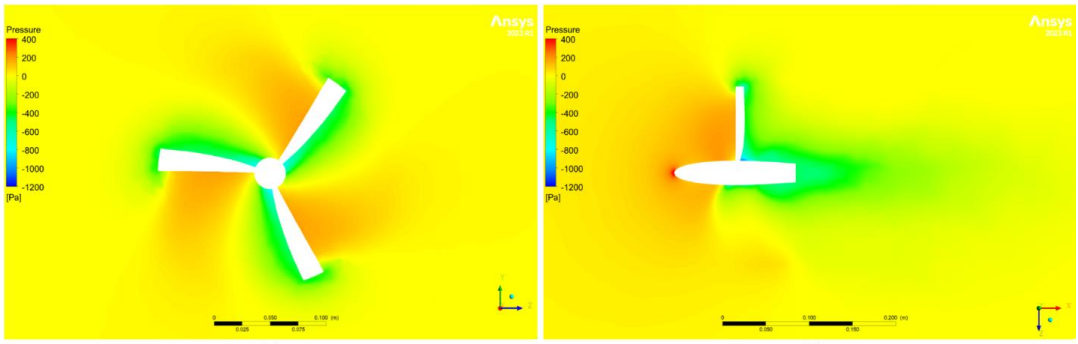

Fig. 8 | Model APFEUP3 - Pressure distribution. (a) Front view. (b) Side view.

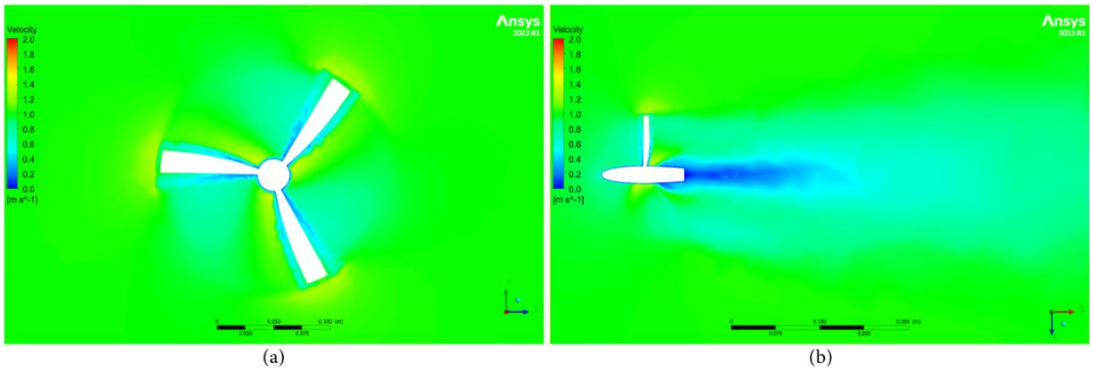

Fig. 9 | Model APFEUP3 - Velocity distribution. (a) Front view. (b) Side view.

By scrutinizing Figure 9a and comparing it with the pressure contour, a correlation is visible between regions of high pressure and low velocity, as well as regions of low pressure and high velocity, consistent with the principles outlined by the Bernoulli's Equation. In Figure 9b, a discernible reduction in flow velocity downstream of the turbine is evident, attributed to the presence of the recirculation zone where the flow tries to recover, due to the interaction with the turbine. This region of lower velocity downstream of the turbine referred to as the wake recovery zone, indirectly affects the performance by modifying the upstream flow conditions, thereby resulting in decreased velocities in the region where the turbine operates. As a result, less kinetic energy is available for extraction. Additionally, the existence of the wake recovery zone often induces turbulence in the flow, which introduces resistance in the turbine, leading to energy losses.

Focusing now on quantitative outcomes concerning the performance of the turbines, Figure 10 shows the power vs. angular velocity curves derived from Computational Fluid Dynamics (CFD) simulations. The data for power and angular velocity values are additionally plotted on the opposite axis for its dimensionless factors, namely the power coefficient (C_P) and tip speed ratio (TSR), respectively.

Through the graph analysis, it is visible that all turbine designs exhibit the expected inverted parabolic shape, with two points of null power: one at null angular velocity and the other at critical speed (null torque). Among the optimized designs, we seek the one with the best performance under established design conditions, specifically a tip speed ratio (TSR) of 1. The comparison of the

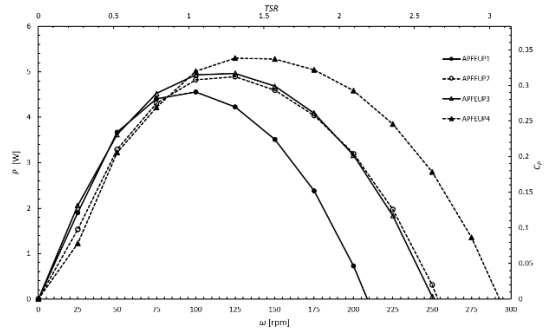

Fig. 10 | Power vs. angular velocity curves for turbine geometries at a water velocity of 1 m/s.

turbine pairs designed with the same hydrofoil, namely APFEUP1-APFEUP2, and APFEUP3-APFEUP4, reveals that an increase in the angle of attack from the first to the second design, respectively, results in wider power curves. This broader curve operates over a wider range of angular velocities and exhibits a higher peak power value. However, a shift of the peak power for a *TSR* value higher than 1, and a decrease in power for lower angular velocities is noticeable.

Among the two hydrofoils employed in the cross-sections, the SG-6043 hydrofoil demonstrates the best performance. The power output variations between the latter compared to the first one for an angle of attack of 0º and an angular velocity of 100 rpm (*TSR* ≈ 1) are 7.8%. Thus, the APFEUP3 and APFEUP4 designs stand out from the rest. The APFEUP3 model was selected between the two options, despite its lower peak power value, as it exhibits differences of 6.8% and 10.8% at lower angular velocities of 75 rpm and 50 rpm, respectively, compared to the APFEUP4 model. Furthermore, the operating speed range of the APFEUP4 design raises structural concerns. Considering the aforementioned factors, the APFEUP3 design is selected for further optimization with the inclusion of the diffuser.

3.1.1. Difuser

Initially, the investigation involved assessing the interaction between flow and diffuser for the studied models. Figure 11a displays the pressure contours, while Figure 11b exhibits the velocity contours for the DFAP2-FEUP diffuser model.

The CFD simulations show the diffuser model converting dynamic pressure into kinetic energy, resulting in increased flow velocity while simultaneously reducing the static pressure. Boundary layer separation was detected within the diffuser resulting in a heightened level of turbu-

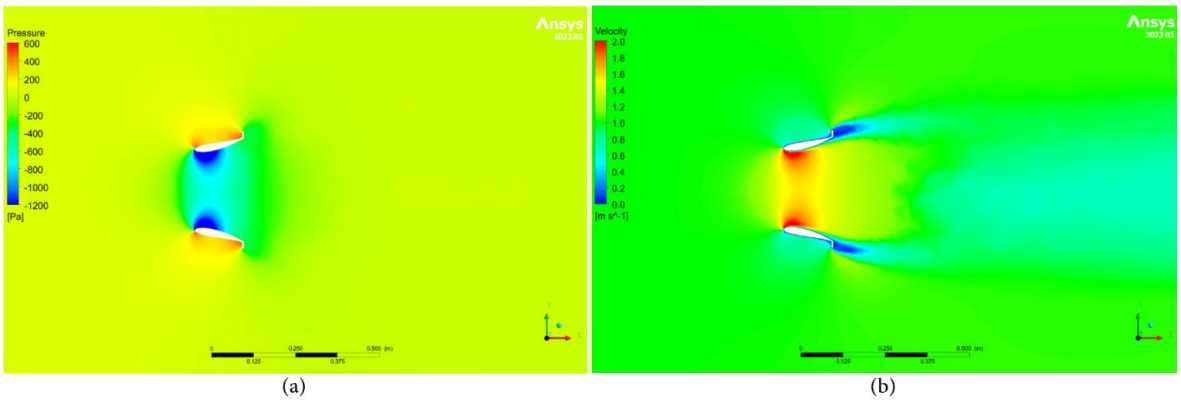

Fig. 11 | DFAP2-FEUP. (a) Pressure distribution. (b) Velocity distribution.

lence, that could potentially impact performance negatively. The implementation of the brim introduces a pressure drop behind the diffuser which creates a suction zone that enhances velocity within the diffuser. Moreover, the brim design helps in minimizing flow losses and re-circulations by controlling fluid expansion and deceleration as it exits the diffuser, maximizing static pressure recovery. Beyond the analysis of the diffuser itself, the examination of the diffuser-turbine assembly is a fundamental aspect of the study. Figures 12 and 13 present the pressure and velocity contours, respectively, for the DFAP2-FEUP model and the turbine.

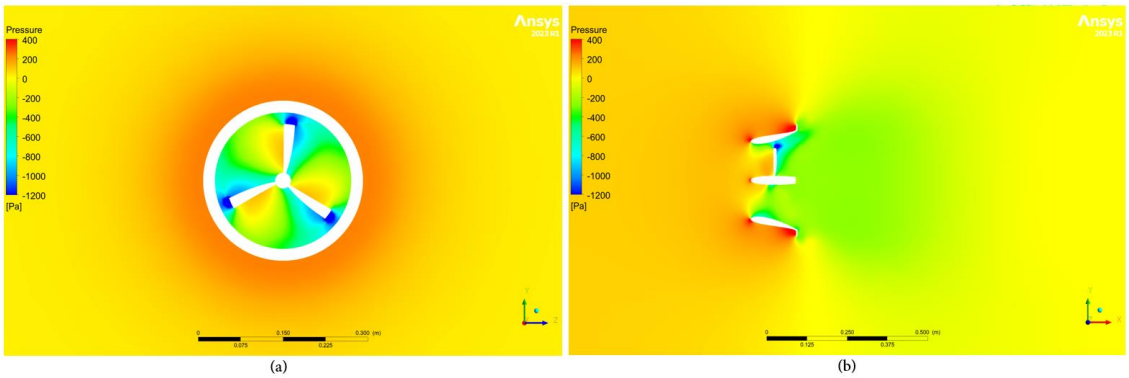

Fig. 12 | Model DFAP2-FEUP with APFEUP3 - Pressure distribution. (a) Front view. (b) Side view.

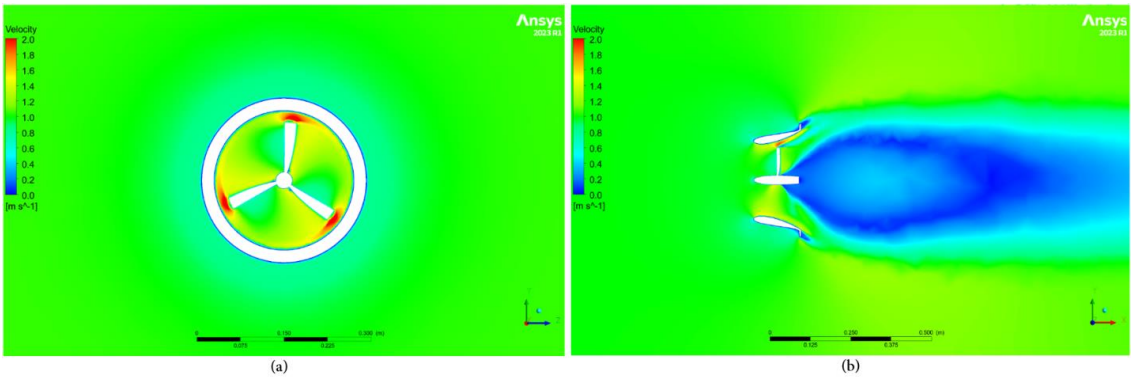

Fig. 13 | Model DFAP2-FEUP with APFEUP3 - Velocity distribution. (a) Front view. (b) Side view.

When comparing Figure 8a with Figure 12a, a notable increment in the pressure difference across the turbine blades (between the high and low-pressure regions) is evident. Additionally, Figure 13a demonstrates a substantial increase in velocity within the diffuser, approximately 45% higher than the velocity observed in Figure 9a. The observed enhancements in pressure distribution and flow velocity illustrate the benefits of implementing a diffuser. However, it is evident, in Figure 13b, an inevitable larger wake zone, which results in an augmented level of turbulence. This wake zone expansion is a noteworthy drawback of the diffuser application. Figure 14 presents the axial velocity profiles at distances of $0D$ (turbine center), $0.35D$, and $3D$ downstream of the turbine for both the bare turbine and the turbine with the diffuser.

A significant reduction in velocity is observed within the wake region, visible at a distance of $0.35D$ and $3D$ from the turbine center. This phenomenon is predominantly attributed to the formation of the recirculation zone. The presence of the diffuser demonstrates more distinct characteristics of vortex generation and velocity dissipation.

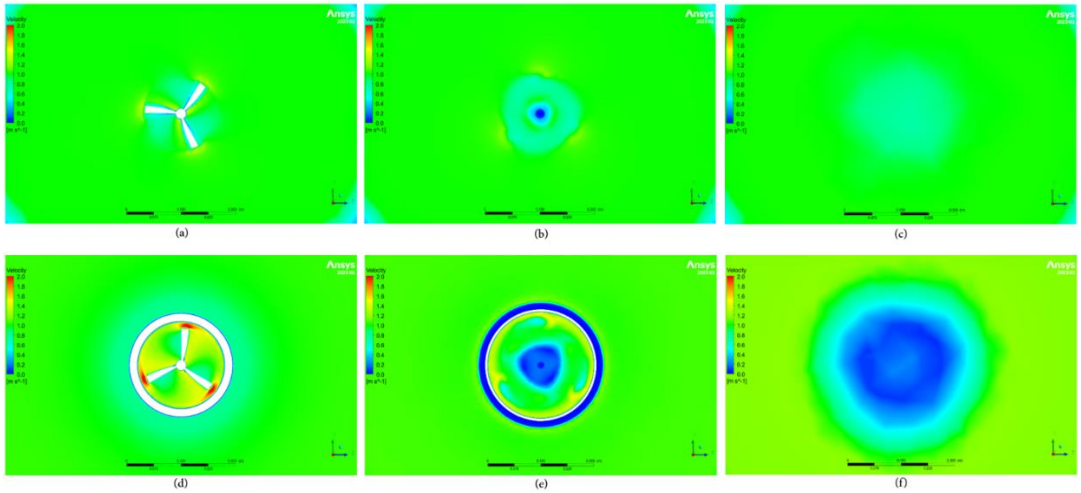

Fig. 14 | Velocity at axial distance: Bare turbine APFEUP3 - (a) 0D; (b) 0.35D; (c) 3D. Diffuser DFAP2-FEUP Implementation - (d) 0D; (e) 0.35D; (f) 3D downstream of the hub center.

Focusing on quantitative results pertaining to the turbine APFEUP3 performance with the implementation of the diffusers, Figure 15 exhibits the power vs. angular velocity curves obtained through Computational Fluid Dynamics (CFD) simulations. Obviously, the curve exhibits resemblances to the one derived for the bare turbines.

The power curve's profile remained consistent, displaying a negative parabolic shape with two zeros, and exhibiting a noticeable power increase throughout the entire curve. When considering the design parameters (angular velocity, $\omega \approx 100$ rpm), the utilization of DFNACA10-FEUP, DFBRIM-FEUP, and DFAP2-FEUP diffusers resulted in power enhancements of 60%, 69%, and 74%, respectively, compared to the APFEUP3 turbine operating independently. Additionally, there was an observed shift of approximately 75 rpm in peak power for most diffusers, since the flow velocity has increased. Notably, the previously mentioned diffuser models demonstrated increases of 83%, 110%, and 111% concerning peak power achieved by the APFEUP3 turbine. The observed enhancements in the extracted power correspond to power coefficients of 57.5%, 66.3%, and 66.5%, respectively, exceeding the *Betz Limit* of 59.3%, particularly in the case of the last two models.

Additionally, the DFBRIM-FEUP and DFAP2-FEUP diffusers exhibited superior performance with power curves indicating higher power values compared to other models.

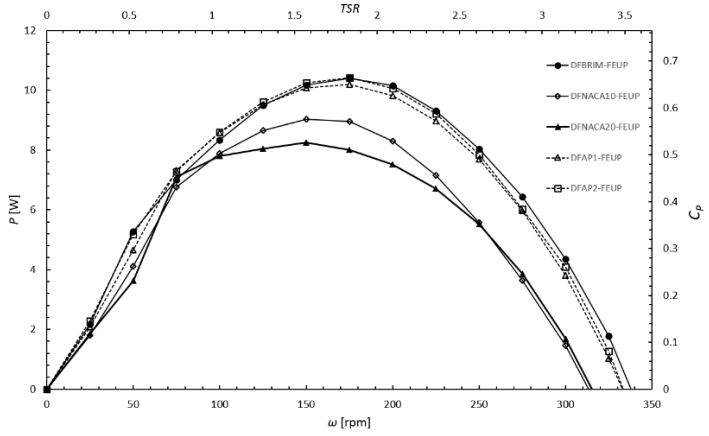

Fig. 15 | Power vs. angular velocity curves for diffuser + turbine geometries.

Nevertheless, it should be emphasized that the DFBRIM-FEUP model was intentionally designed with larger dimensions than the other diffuser models, in order to obtain higher power values for subsequent comparison purposes. Consequently, the DFAP2-FEUP diffuser, which practically matches the power curve of the previous one, was selected for further advancement into the construction phase. It should be noted that the DFAP2-FEUP design was among those developed in the study, demonstrating significant advancements in the implementation of diffusers to increase the efficiency of hydrokinetic turbines. Moreover, this study can serve as a promising basis for further research and developments in this domain. Finally, the turbine support was incorporated into the DFAP2-FEUP model. After integrating the support structure, a 14% reduction in peak power performance was observed, as expected. The incorporation of the support is intended to be improved in future work. Subsequently, the predictions of the model were subjected to verification and validation through laboratory experiments.

3.2. Experimental characterization

Finally, empirical findings were acquired and juxtaposed with the results from the numerical model. The evaluation encompassed the experimental analysis of the assembly involving turbine APFEUP3 and diffuser DFAP2, singled out for their superior overall efficiency. The graphical representation in Figure 16 delineates the comparison of power coefficient (C_P) against tip speed ratio (*TSR*) for both experimental and numerical models. Notably, both the experimental set-up and the CFD model incorporated the support to secure the turbine. The laboratory experiment results embraced the inherent uncertainty associated with power coefficient and tip speed ratio measurements. However, it was determined that this uncertainty had a minimal influence on the observed disparities.

Upon comparing the experimental outcomes with the Computational Fluid Dynamics (CFD) model, a discernible disparity becomes evident. Nevertheless, it is perceptible that the experimental curve conforms to the anticipated parabolic shape and both curves manifest the peak power at an angular velocity of approximately 15 rpm. However, a significant discrepancy of approximately 32.5% in peak power is evident when comparing the results from the CFD model and the experimental data.

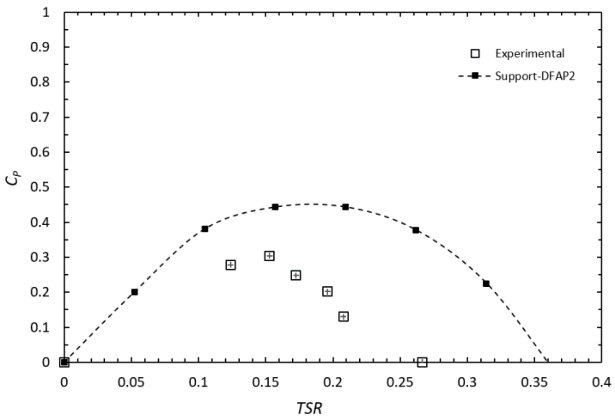

Fig. 16 | C_P vs. *TSR* curve for experimental set-up and Support-DFAP2-FEUP diffuser numerical model assembly at a water velocity of 0.11931 m/s.

When considering the divergences between the numerical model results and the experimental observations, a multitude of plausible explanations emerge. For instance, the CFD model assumes certain simplifications dictated by the intricate dynamics of fluid motion and the computational complexities involved. These simplifications could potentially contribute to an overestimation of model results vis-à-vis experimental data. Additionally, it is imperative to acknowledge the utilization of only one turbulence model, neglecting the possibility that alternative turbulence models might yield disparate outcomes.

Furthermore, constrained by computational resources, the CFD simulations applied to the turbine-diffuser assemblage necessitated substantial computational effort, thereby restricting the capacity to investigate a diverse array of model configurations. The prototype employed in this study is not devoid of imperfections. Primary disparities are likely attributed to the prototype's construction, notably the inevitable friction encountered along the rotational axes due to the presence of the four bearings and the pair of bevel gears, indispensable for testing within the existing conditions. Remarkably, adding a mass of 30 grams, for instance, to the experimental results, aimed at offsetting axis-related friction, yields results that closely align with the numerical model predictions. Moreover, it is imperative to acknowledge that the velocity profile upstream of the turbine diverges significantly from the assumed constant profile within the CFD model.

Hence, judiciousness is imperative when examining the experimental outcomes, acknowledging that they cannot be regarded as absolute certainties but rather as indicative approximations of turbine performance.

4- CONCLUSION

The primary aim of this research was to design and optimize a portable horizontal axis hydrokinetic turbine capable of extracting energy from water flows, such as rivers and canals. The focus was on enabling portability, making it suitable for easy transportation. In comparison to wind and solar energy sources, hydrokinetic turbines offer advantages due to their consistent stability throughout the day and year, making them operable at any time. To maximize energy extraction and attain high power coefficients (C_P), lift-based hydrokinetic turbines were selected, effectively converting the kinetic energy of flowing water into mechanical energy. These turbines are limited by the *Betz Limit*, a fundamental theoretical threshold setting the maximum energy conversion efficiency at 59.3% for bare turbines.

The *QBlade* software was employed to determine the chord and twist angle values for each section of the turbine blade using the *Blade Element Momentum* (BEM) theory. For the blade design, two hydrofoils were used for the cross-section, namely, Eppler 817, and SG-6043, testing two angles of attack for each hydrofoil. The twist angle was optimized based on the quotient between the lift and drag coefficients, while the chord values were optimized

considering a target tip speed ratio (*TSR*) of 1, a turbine diameter of 20 cm, and a water velocity of 1 m/s, commonly found in rivers with low gradients.

A numerical model was developed using *ANSYS* R1 2023 software to assess the performance of the turbine models. Power vs. angular velocity curves were generated using the torque values obtained from steady-state simulations, where the pressure and viscous forces acting on the turbine blades were integrated. Among the designed turbine models, the APFEUP3 model optimized for SG-6043 hydrofoil at an angle of attack of 0º exhibited the most promising performance, achieving a maximum power coefficient of 31.7% at the design *TSR*. Furthermore, the feasibility of incorporating a diffuser around the APFEUP3 turbine was investigated to enhance flow velocity and, consequently, improve the turbine's performance. The diffuser was designed with a diameter of 35 cm and a length of 15 cm, due to portability constraints. Turning to the optimization study of the diffuser geometry, several noteworthy conclusions emerge. The implemented diffuser models significantly increased flow velocity and pressure difference across the turbine blades, resulting in notable power improvements. The DFAP2-FEUP, a custom-designed diffuser, allowed the best turbine performance, reaching a maximum power coefficient of 66.5%, surpassing the *Betz Limit*. Lastly, integrating the support structure, which positioned the turbine in the center of the diffuser, led to a 14% reduction in the maximum extracted power.

The experimental prototype was subjected to rigorous testing to replicate the power vs. angular velocity curve obtained from the numerical model. The resistive torque, applied by a conventional generator to the turbine's shaft, was emulated by a rigidly connected wire with a mass, which generated a torque opposing the torque produced by the turbine. The obtained experimental results exhibited a discrepancy of approximately 32.5% in peak power compared to the numerical model. These variations could be attributed to various factors, such as simplifications and approximations used in the model, the choice of turbulence model, as well as operational challenges encountered during the testing phase. The primary attributive factor for the observed disparities in the results is attributed to frictional effects occurring on the rotating shafts, notwithstanding their fabrication with the intention of friction reduction. It is crucial to acknowledge that the assembled prototype may have inherent imperfections, which implies that the experimental findings should not be regarded as absolute truths but rather as indicative values.

ACKNOWLEDGMENTS

Authors gratefully acknowledge the Faculty of Engineering of the University of Porto (FEUP), the Department of Mechanical Engineering (DeMEC) of FEUP, the Institute of Science and Innovation in Mechanical and Industrial Engineering (LAETA-INEGI), and the Centre for Nanotechnology and Smart Materials (CeNTI).

REFERENCES

[1] D. K. Okot, "Review of small hydropower technology," Renewable and Sustainable Energy Reviews, vol. 26, pp. 515–520, 2013, issn: 13640321. doi: 10.1016/j.rser. 2013.05.006.

[2] A. Rodrigues, HYDROPOWER I, Generalities, Maturity of the technology and hydropower contribution, Brief historical notes, Energy and hydropower, Classification of hydropower plants, Elements of civil works, Hydraulic circuit, Notas das aulas de Energias Renov´aveis II, 2022.

[3] A. H. Elbatran, M. W. Abdel-Hamed, O. B. Yaakob, Y. M. Ahmed, and M. A. Ismail, "Jurnal teknologi hydro power and turbine systems reviews," Tech. Rep., 2015, pp. 2180–3722. [Online]. Available: www.jurnalteknologi.utm.my.

[4] E. Chica and A. Rubio-Clemente, Design of Zero Head Turbines for Power Generation. InTech, Jul. 2017. doi: 10.5772/66907.

[5] A. Kumar and R. P. Saini, "Performance parameters of savonius type hydrokinetic turbine - a review," Renewable and Sustainable Energy Reviews, vol. 64, pp. 289–310, Oct. 2016, issn: 18790690. doi: 10.1016/j.rser.2016.06.005.

[6] S. La´ın, L. T. Contreras, and O. L´opez, "A review on computational fluid dynamics modeling and simulation of horizontal axis hydrokinetic turbines," Journal of the Brazilian Society of Mechanical Sciences and Engineering, vol. 41, 9 Sep. 2019, issn: 18063691. doi: 10.1007/s40430-019-1877-6.

[7] M. Barbari´c and Z. Guzovi´c, "Investigation of the possibilities to improve hydrodynamic performances of micro-hydrokinetic turbines," Energies, vol. 13, 17 Sep.2020, issn: 19961073. doi: 10.3390/en13174560.

[8] A. C. B. Junior, R. C. Mendes, T. Wirrig, R. Noguera, and T. F. Oliveira, "On the design of propeller hydrokinetic turbines: The effect of the number of blades,"Journal of the Brazilian Society of Mechanical Sciences and Engineering, vol. 41, 6 Jun. 2019, issn: 18063691. doi: 10.1007/s40430-019-1753-4.

[9] I. Badea, M. G. Cojocaru, M. V. Pricop, and A. Bobonea, "Design procedure and numerical analysis of a small horizontal-axis hydrokinetic turbine," U.P.B. Sci. Bull., Series D, vol. 76, 3 2014, issn: 1454-2358.

[10] C. hee Jo, J. young Yim, K. hee Lee, and Y. ho Rho, "Performance of horizontal axis tidal current turbine by blade configuration," Renewable Energy, vol. 42, pp. 195–206, Jun. 2012, issn: 09601481. doi: 10.1016/j.renene.2011.08.017.

[11] H. N. Wu, L. J. Chen, M. H. Yu, W. Y. Li, and B. F. Chen, "On design and performance prediction of the horizontal-axis water turbine," Ocean Engineering, vol. 50, pp. 23–30, Aug. 2012, issn: 00298018. doi: 10.1016/j.oceaneng.2012.04.003.

[12] K. A. Aganah, B. Pokharel, and O. Ojo, "The steady-state interaction of a gridconnected doubly-fed induction generator and the wind turbine," 2011, pp. 2657–2663, isbn: 9781457705427. doi: 10.1109/ECCE.2011.6064124.

[13] L. A. Gish and G. Hawbaker, "Experimental and numerical study on performance of shrouded hydrokinetic turbines," OCEANS 2016 MTS/IEEE Monterey, OCE 2016, Nov. 2016. doi: 10.1109/OCEANS.2016.7761041.

[14] W. D. C. S. J. R. Z. A. K. A. Oztekin and R. C. Klein, "Design and simulation of a micro hydrokinetic turbine,"

[15] B. Freedom, Blue Freedom Portable. Web Page, [Online]. Available: https : // bestfriendportable.clickmake.com/hydro/portable/, 2023.

[16] W. Lily, WaterLily Turbine. Web Page, [Online]. Available: https : / / shop. waterlilyturbine.com/products/waterlily-turbine, 2023.

[17] J. M. R. C. B. Francisco Mira Piteira Espenica Ricardo Balbino dos Santos Pereira, "Design and optimization of hydrofoils tailored for marine current turbines," Tech.Rep., 2018.

[18] D. Marten and J. Wendler, "Qblade guidelines v0.6," Tech. Rep., 2013.

[19] J. H. Lee, S. Park, D. H. Kim, S. H. Rhee, and M.-C. Kim, "Computational methods for performance analysis of horizontal axis tidal stream turbines," Applied Energy, vol. 98, pp. 512–523, 2012, issn: 0306-2619. doi: https://doi.org/10.1016/j.apenergy.2012.04.018.

[20] M. Shives and C. Crawford, "Developing an empirical model for ducted tidal turbine performance using numerical simulation results," Proceedings of the Institution of Mechanical Engineers, Part A: Journal of Power and Energy, vol. 226, pp. 112–125,1 2012, issn: 20412967. doi: 10.1177/0957650911417958.